Proc. Natl. Acad. Sci. USA
Vol. 95, pp. 11065–11070, September 1998
Biochemistry

The 2.8-Å structure of rat liver F_1-ATPase: Configuration of a critical intermediate in ATP synthesis/hydrolysis

(ATP synthase/F_oF_1-ATPase/oxidative phosphorylation/mitochondria/x-ray diffraction)

MARIO A. BIANCHET*, JOANNE HULLIHEN†, PETER L. PEDERSEN†, AND L. MARIO AMZEL*‡

Departments of *Biophysics and Biophysical Chemistry and †Biological Chemistry, The Johns Hopkins University School of Medicine, 725 North Wolfe Street, Baltimore, MD 21205-2185

Communicated by William A. Catterall, University of Washington School of Medicine, Seattle, WA, July 9, 1998 (received for review April 3, 1998)

ABSTRACT **During mitochondrial ATP synthesis, F_1-ATPase—the portion of the ATP synthase that contains the catalytic and regulatory nucleotide binding sites—undergoes a series of concerted conformational changes that couple proton translocation to the synthesis of the high levels of ATP required for cellular function. In the structure of the rat liver F_1-ATPase, determined to 2.8-Å resolution in the presence of physiological concentrations of nucleotides, all three β subunits contain bound nucleotide and adopt similar conformations. This structure provides the missing configuration of F_1 necessary to define all intermediates in the reaction pathway. Incorporation of this structure suggests a mechanism of ATP synthesis/hydrolysis in which configurations of the enzyme with three bound nucleotides play an essential role.**

In mitochondria and bacteria, the ATP synthase complex (F_0F_1) uses the electrochemical proton gradient generated by the respiratory chain to produce ATP at the concentrations needed for cellular functions. Homologous proteins produce ATP in chloroplasts by using the proton gradient generated during photosynthesis. The mechanism by which ATP synthase couples the proton gradient to the synthesis of ATP remains one of the central questions in bioenergetics. The F_1 sector, the portion of the enzyme that contains the nucleotide binding and catalytic sites, can be isolated as a soluble multiple subunit protein ($\alpha_3\beta_3\gamma\delta\varepsilon$, molecular weight is ≈371,000; refs. 1 and 2) that exhibits ATPase activity (F_1-ATPase). The lengths of the subunits in the rat liver enzyme are as follows: α, 510 residues; β, 479 residues; γ, 270 residues; δ, 142 residues; and ε, 50 residues. In negatively stained micrographs, the rat liver enzyme appears as six regions in an hexagonal arrangement surrounding a central mass (3). During ATP synthesis, the F_1 sector undergoes concerted conformational changes (the "binding change mechanism"; for reviews see references 4–8) that couple changes in the nucleotide binding sites of the β subunits with rotations of the γ subunit (9–14). Understanding the nature of these structural changes is essential for understanding ATP synthesis. In this paper, we report the structure of a native form of rat liver F_1-ATPase crystallized by precipitation with ammonium sulfate from a buffer used for the determination of ATPase activity: 5 mM ATP and 200 mM potassium phosphate (pH 7.2) (15). Mg^{2+} was omitted from the buffer to prevent immediate hydrolysis of the ATP in the crystallization media.

The structure of bovine heart F_1-ATPase crystallized from a 20 mM $MgSO_4$ solution containing the inhibitors 5′-adenylyl-β,γ-imidodiphosphate (250 μM), ADP (5 μM), and azide (0.02% wt/vol) has been reported (14, 16). This structure (hereafter the "two-nucleotide structure") contains nucleotides in only two of the three β subunits; the empty subunit has a substantially different conformation from the other two, which are distinct but similar to each other (Fig. 1). This marked asymmetry was proposed to be an intrinsic property of the enzyme (14). The structure of rat liver F_1-ATPase crystals reported here ("three-nucleotide structure"), grown in the presence of substantially higher, more physiological concentrations of nucleotides, contains nucleotides in all three β subunits and has all β subunits in highly similar conformations (Fig. 1). This structure, with all catalytic and noncatalytic sites occupied by nucleotide, is a form of the enzyme that provides the missing configuration of F_1 necessary to define all intermediates in the reaction pathway of ATP synthesis. Inclusion of this additional, key configuration results in significant modifications to previously proposed mechanisms.

MATERIALS AND METHODS

Preparation and Characterization of the Crystals. The protein was purified and crystallized by ammonium sulfate precipitation in 200 mM KP_i plus 5 mM ATP (pH 7.5) as described (15, 17). Crystals of F_1 were dissolved in 50 μl of 250 mM KP_i plus 5 mM EDTA (pH 7.5), and 15 μg were subjected to SDS/PAGE in cylindrical gels. After staining with Coomassie blue, gels were scanned by using a scanning attachment on a Gilford spectrophotometer. To determine the capacity of redissolved crystals to rebind to F_1-depleted inner membrane vesicles of mitochondria and to regain sensitivity to oligomycin, an inhibitor of oxidative phosphorylation, purified F_1 (200 μg) in 250 mM KP_i plus 5 mM EDTA (pH 7.5) was reconstituted with F_1-depleted inner membrane vesicles (0.5 mg) of rat liver mitochondria in a 0.1-ml system at 25°C. Inner membrane vesicles and F_1-depleted inner membrane vesicles were prepared as described (18). Inhibition was measured in the presence of 1 μg of oligomycin. To determine the relative capacity of ATP and $MgCl_2$ to initiate the F_1 ATPase reaction, kinetic measurements were made initiating the reaction either with 4 mM ATP or with 4.8 mM $MgCl_2$. ATPase activity was assayed by coupling the formation of ADP to the pyruvate kinase and lactic dehydrogenase reactions as described (18). The decrease in optical density of NADH at 340 nm was monitored.

Structure Determination. All data were collected at 100 K on an R-Axis II Image Plate System (Molecular Structure, The Woodlands, TX) operating on a Rigaku RU200 generator implemented with a graphite monochromator. Crystals were stabilized for freezing by the addition of glycerol (33–35%, wt/vol) to the mother liquor. Typically, 60° of data were collected from a single crystal that yielded complete data sets with high redundancy. To check the symmetry, one set of 200° of data was collected and processed in space group P1, in three different orientations of C2, and in R32. Data were processed by using the program DENZO (19) and were scaled by using SCALEPACK (19).

The publication costs of this article were defrayed in part by page charge payment. This article must therefore be hereby marked "*advertisement*" in accordance with 18 U.S.C. §1734 solely to indicate this fact.

Data deposition: The atomic coordinates have been deposited in the Protein Data Bank, Biology Department, Brookhaven National Laboratory, Upton, NY 11973 (PDB ID Code 1MAB).

‡To whom reprint requests should be addressed. e-mail: mario@neruda.med.jhmi.edu.

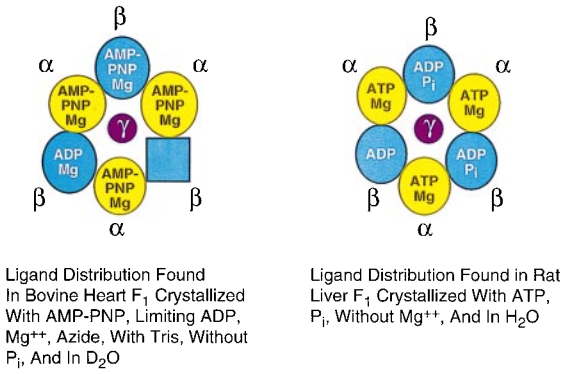

FIG. 1. Schematic representation of the crystallization conditions and the bound nucleotides in the two-nucleotide structure (*Left*, bovine heart, ref. 14) and the "three-nucleotide structure" (*Right*, rat liver, this work).

The possibility of twinning was checked by calculating the ratio $\langle F\rangle^2/\langle F^2\rangle$ (20). All heavy atom calculations were carried out with the CCP4 suite of programs (21). Heavy atom positions were estimated from difference Patterson maps. Different heavy atom derivatives were placed on the same origin either by the presence of common sites or by the use of difference Fourier maps. Refinement of heavy atom positions and phase calculations were performed with the program MLPHARE as implemented in CCP4. Phase improvement through density modification was carried out with the program DM as implemented in CCP4. Interpretation of the maps and building of the atomic models were carried out with the program O (22). One α subunit, one β subunit, and part of one γ subunit were built. The γ subunit, present in one-third copy per asymmetric unit, was built by using maps contoured at densities about one-half the density level used to contour the rest of the map. Models were refined with the program XPLOR (23). Cycles of gradient refinement were followed by runs of simulated annealing using slow cooling. After convergence, the model was checked against the original map, 2Fo-Fc maps, and maps using phases and weights obtained by a combination of experimental and calculated phases by using the program SIGMAA as implemented in CCP4. When necessary, sections of the model were rebuilt by using the program O. Special attention was given to trying to identify regions that could be built in more than one conformation, reflecting different conformations in the three copies of the major subunits. In the final cycles, the occupancies of the ADP and the P_i were refined independently. Geometrical and conformational parameters of the final model were checked with the program PROCHECK as implemented in CCP4. Molecular drawings were done by using SETOR (24) and MOLSCRIPT (25) and RASTER3D (26, 27)

RESULTS AND DISCUSSION

Biochemical Characterization of the Crystals. Crystals of rat liver F_1-ATPase (Fig. 2*A*), obtained as described (15), were analyzed to ascertain that the crystallized protein was still native and fully active. The crystallized material, dissolved by addition of ammonium sulfate-free crystallization buffer, contained all five subunits (Fig. 2*B*), was able to hydrolyze ATP and to restore oligomycin sensitive ATPase activity to F_1-depleted inner mitochondrial membranes (Fig. 2*C*). The physiological relevance of the crystallization conditions was ascertained by showing that addition of Mg^{2+} to an F_1 plus ATP solution or addition of ATP to an F_1 plus Mg^{2+} solution yields indistinguishable kinetics (Fig. 2*D*), indicating that, in our crystallization conditions, the F_1-ATP complex is poised for ATP hydrolysis: release of bound ATP is not a prerequisite to the formation of bound ATP-Mg^{2+}; that is, Mg^{2+} can bind directly to F_1-bound ATP to initiate hydrolysis.

Crystal Symmetry. The rat liver F_1-ATPase crystals, space group R32 (17) (Table 1), contain two F_1 molecules in the unit cell, and therefore, in the asymmetric unit of the crystal, there is

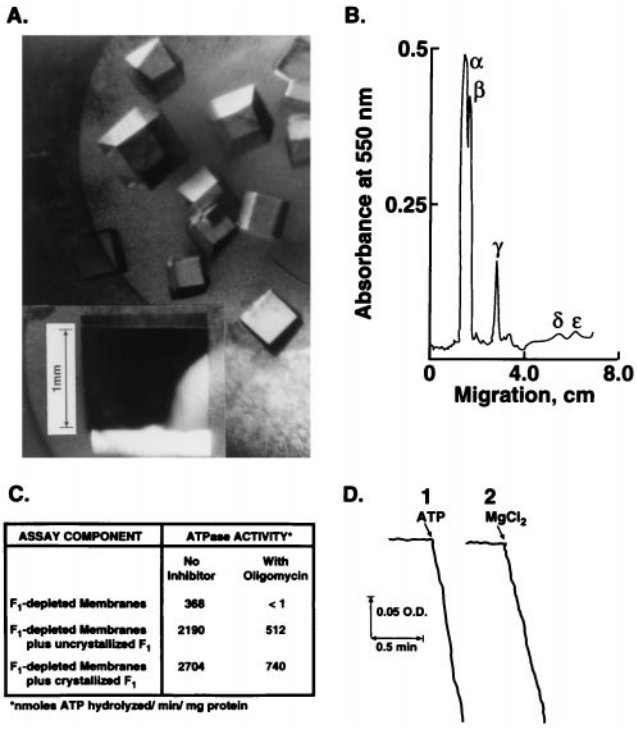

FIG. 2. (*A*) Diffraction quality crystals of rat liver F_1. (*B*) Scan of an SDS/PAGE gel of redissolved F_1 crystals. Crystals of F_1 were dissolved in 50 μl of 250 mM KP_i plus 5 mM EDTA (pH 7.5), and 15 μg were subjected to SDS/PAGE in cylindrical gels. (*C*) Capacity of redissolved crystals to rebind to F_1-depleted inner membrane vesicles of mitochondria and regain sensitivity to oligomycin, an inhibitor of oxidative phosphorylation. Where indicated, 1 μg oligomycin was present. (*D*) Relative capacity of ATP and $MgCl_2$ to initiate the F_1 ATPase reaction. The decrease in optical density of NADH at 340 nm was monitored. Reaction 1 was initiated with 4 mM ATP, and reaction 2 was initiated with 4.8 mM $MgCl_2$.

one-third of one F_1 molecule ($\alpha\beta\gamma_{1/3}\delta_{1/3}\varepsilon_{1/3}$). Because this is an unusual result, the symmetry and space group assignments were checked thoroughly during different stages of the structure determination by using many different schemes. For example, a complete data set was collected in space group P1 (10^6 observations). Processing of these data in space group R32, in the three different possible orientations of C2 (subgroups of R32), and in P1 showed no significant differences in R_{sym} (corrected by multiplicity) even in the outer shells. In addition, the possibility of twinning was ruled out based on the ratio $\langle F\rangle^2/\langle F^2\rangle$ (20). The value obtained for the acentric data is indicative of an untwinned crystal. Based on these and similar results, we carried out all calculations in space group R32.

Map Interpretation. The multiple isomorphous replacement electron density map (Table 1) showed interpretable density for the α and β subunits and parts of the γ subunits (sequences in refs. 28 and 29), as well as density for the bound nucleotides. As in the bovine heart structure (14), no interpretable density was found for the two smallest subunits, δ and ε.

The single α and β subunits in the asymmetric unit of the crystals represent a superposition of the three copies present in an F_1 molecule. With the exception of a small number of localized regions, the electron density of the α and β subunits in the asymmetric unit are well defined, evidencing that, in the three-nucleotide structure, the three α subunits and the three β subunits are in very similar conformations (Fig. 3) (30, 31). In a small number of places, the density shows that the chain is present in more than one conformation. These alternative conformations probably represent minor differences among the three copies of

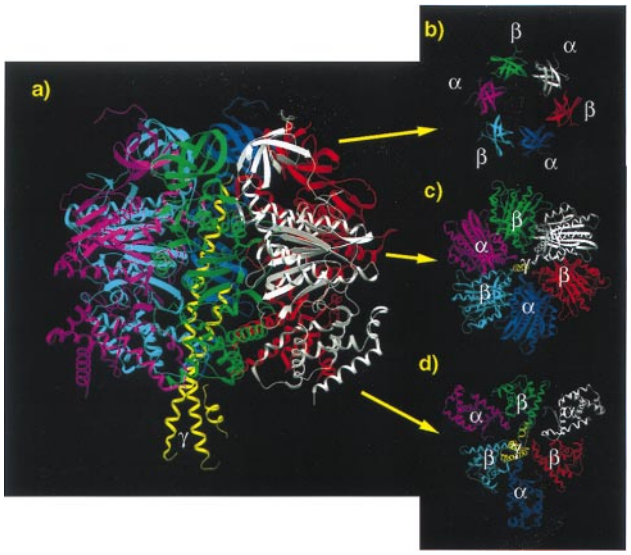

FIG. 3. Ribbon diagram of the rat liver F_1-ATPase. Rat liver F_1 can be described as an "inverted apple" 110 Å in diameter and 125 Å in length (including the protruding γ subunit) formed by three α and three β subunits alternating around the 3-fold axis of symmetry of the R32 cell, in agreement with the 3.6-Å resolution structure reported (17). The molecule is most narrow at the "top," where a depression surrounding the 3-fold axis marks the beginning of a large central channel partially occupied by the γ subunit. Parts of the γ subunit extend well beyond the end of the major subunits, forming a long narrow protrusion (the "stem" of the apple). This side, the "bottom" of the F_1, is thought to be closest to the membrane in the F_0F_1 complex. (*a*) "Side view" of complete model (viewed from a direction perpendicular to the 3-fold axis).The α and the β subunits are also alike, both composed of three domains: an NH_2-terminal β sheet domain, a nucleotide binding domain, and a COOH-terminal domain. (*b*) "Top view" of the NH_2-terminal domain. (*c*) Top view of the nucleotide binding domain. (*d*) Top view of the COOH-terminal domain. In the top views (*c* and *d*) the corresponding portions of the γ subunit are shown in yellow.

the major subunits in the F_1 molecule. The F_1 molecule shown in Fig. 3 has three $\alpha\beta$ pairs related by a 3-fold axis of symmetry.

Description of the Structure. The structure of the α subunits is highly similar to those of the bovine heart crystals, both with respect to conformation and to nucleotide content. However, significant differences exist between the two structures in one of the β subunits. In the two-nucleotide structure (14), the β subunits are present in three different conformations: tight (T), loose (L), and open (O), containing 5′-adenylyl-β-γ-imidodiphosphate (β_T), ADP (β_D), or no nucleotide (β_E), respectively (Fig. 1). Subunits β_T and β_D are alike, but the one in the β_E, open conformation differs from the other two by a large hinge motion of the carboxy terminal domain (some portions move >20 Å). In contrast, all β subunits in the three-nucleotide structure are in similar conformations, analogous to β_D or β_T of the two-nucleotide structure. There is no indication of an open conformation in the crystals reported here. The rms deviations for all atoms of the β subunit nucleotide binding domain in the three-nucleotide structure with respect to the β_T and the β_D subunits of the two-nucleotide structure are 0.81 Å and 0.88 Å, respectively. The equivalent rms deviation between the β_T and the β_D subunits of the two-nucleotide structure is 0.30 Å. The main cause of the difference between the two structures (i.e., the presence of an open conformation in one and not in the other) appears to be the absence of nucleotide in one of the subunits of the bovine heart crystals. Significantly, recent experiments (32) have shown that, under physiological concentrations of nucleotides, F_1 molecules in solution have bound nucleotides in all three β subunits. The correlation between the open conformation and absence of nucleotide was confirmed by the structure of an $\alpha_3\beta_3$ complex from a thermophilic bacterium. This structure, determined in the absence of nucleotides, has all β subunits in the open conformation (33).

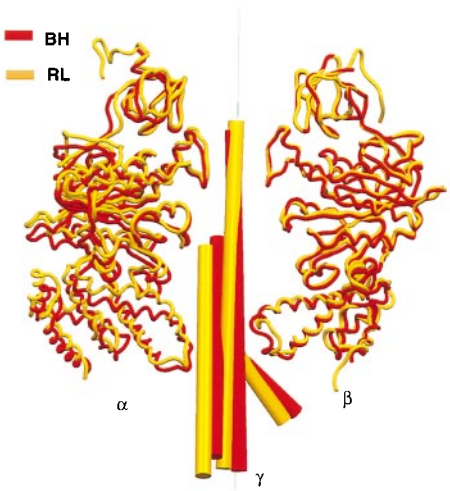

FIG. 4. Differences in position of the γ subunit between the rat liver and the bovine heart enzyme. The lower part of the γ subunit in rat liver F_1 (gold) is displaced from the central axis ≈4 Å more than the bovine heart γ subunit (red); bovine heart subunits β_{TP}/α_E (opposite subunit pair) were used as references for alignment.

The electron density maps show low but interpretable density for three regions of the γ subunit. Phasing the sequence to the observed density was aided by the information available from the two-nucleotide structure (14). Because of crystal symmetry, the regions of γ visible in the rat liver crystals are seen as three partially occupied overlapping copies. Nevertheless, by using a low electron density contour level, large portions of the subunit were interpretable. Only one of the three partially overlapping copies was built and included in the refinement at one-third the occupancy because the other two copies are generated by symmetry. It is possible for an asymmetric unit to contain one-third of a nonsymmetrical subunit if the unit cell contains three equivalent sites for the subunit, but only one of the three is occupied in any one cell. Under these conditions, the individual cells do not possess 3-fold symmetry, but the crystal does. The sections of the γ subunit built consist of three stretches of α-helix (Fig. 3); two of these helices (residues 1 to 41 and 206 to 270) form an antiparallel coiled-coil that runs parallel to the 3-fold axis; the other (residues 74 to 87) forms a short rod that extends outward, making an angle of ≈60° with the coiled-coil (Fig. 3). All three regions have interactions with the major subunits. Some of these contacts are also present in the two-nucleotide structure (14). However, alignment of the two structures shows that the positions and orientations of their γ subunits differ considerably. A small difference in the conformation of the γ subunit results in a 4-Å translation (the rat liver further from the center; Fig. 4). This change affects contacts of γ with the major subunits, especially the interactions with the loop containing the DELSEED sequence. The functional implications of these contacts are discussed below.

The α and β subunits make extensive contacts with each other (area buried in the α plus β interface is 4, 672 $Å^2$ per interface; 3,009 $Å^2$ apolar, 1, 663 $Å^2$ polar) but, neither α-α nor β-β contacts are present in the structure. The nucleotide binding sites occur at subunit interfaces.

Nucleotide Binding Sites. In the β subunit, the maps showed well defined electron density for the adenine, the ribose, and the α and β phosphates. A large density separated from the β phosphate was interpreted as indicating the presence of P_i. To determine whether all β subunits contained bound nucleotides and/or P_is, the occupancies of the ADP and of the P_i were allowed to vary during the last stages of the refinement. Care was taken to ensure that refined occupancies remained as independent as

Table 1. Summary of crystallographic analysis

Crystals				
Rhombohedral; space group R32				
Cell dimensions, hexagonal: $a = b = 143.67$ Å, $c = 361.15$ Å, $z = 6$				
Data collection and heavy atom refinement				
	Native	$Hg(CN)_2$	$Hg(NO_3)_2$	Ethyl HgCl
Number of reflections	35334	17715	13946	37758
Resolution	2.8	3.5	4.5	2.8
R_{sym}	10.3	11.0	13.0	13.0
Completeness, %	85.3	82.4	67.0	97.2
$I/\sigma_{(I)}$, in last shell	7.1	5.0	5.2	6.0
Fractional ΔF ($\Delta F/F$)		0.14	0.14	0.19
Number of sites		1 (2)	2	1
R_{Cullis}		0.83	0.96	0.83
Phasing				
Average figure of merit				
Multiple isomorphous replacement			0.34	
After density modification			0.98	
Refinement				
Number of reflections	24,958	(6–2.8Å; $I > 3\sigma$)		
Number of atoms	8,492	(66 waters)		
R (R_{free})	0.217	(0.290; test set 2.5% of data)		
rms deviation from ideality				
Bond lengths	0.013 Å			
Bond angles	2.08°			
Improper angles	1.73°			
Temperature factors, average	49 Å^2			
Models	Number of residues		Built	
α subunits	510		10–510	
β subunits	479		1–477	
γ subunits	270		1–45, 74–87, 206–270	

possible of temperature factors. With the temperature factors of the nucleotide atoms set to the average value of the surrounding atoms, nucleotide occupancies were allowed to vary during 200 cycles of positional refinement. The occupancies were then fixed at the refined values, and the temperature factors were refined to convergence. The final temperature factors of the nucleotide atoms remained similar to those of surrounding protein atoms. The occupancy of the ADP refined to a value close to 1.0 (1.04) and that of the P_i refined to a value close to 0.66 (0.70), indicating that all three β subunits contain bound ADP and two contain, in addition, bound P_i. These results confirm our previous observation that, when ATP is present in the medium, three moles of ADP per mole of F_1 are bound (34). The nucleotides are in the anticonformation, and the sugar pucker is C3′ endoconformation (Fig. 5*A*). Although the crystallization medium contained only ATP and no Mg^{2+}, low ATPase activity in the absence of Mg^{2+} ions and nonenzymatic hydrolysis of ATP produced the ADP during the crystallization period (2 weeks to several months). Main chain (residues 158 to 165, the P-loop) and side chain groups (including Arg-373 from α) participate in hydrogen bonds to the ribose, the diphosphate, and the P_i (Fig. 5 *A*, *C*, and *D*). Glu 188 is hydrogen-bonded to an oxygen of the P_i in a position that makes it a strong candidate to participate directly in ATP synthesis: it can provide the proton for the abstraction of the water. Conversely, in ATP hydrolysis, it may function as the catalytic base (14).

Comparison of the nucleotide binding site of the three-nucleotide structure (ADP and P_i but no Mg^{2+}) with the β_T subunit (5′-adenylyl-β-γ-imidodiphosphate-Mg^{2+}) of the two-nucleotide structure (Fig. 5*C*) shows that Mg^{2+} binding between Thr 163 and the phosphates pushes the β and γ phosphates farther away from the P-loop, allowing a water molecule to bind to Glu 188. Only small differences of <0.8 Å exist between the positions of some of the atoms in the P-loop of the two structures (Fig. 5*C*), indicating that Mg^{2+} binding to ATP in the β subunits causes no major conformational changes. Thus, the main difference between the structures of the F_1-ATPase in the bovine heart and the rat liver crystals—the presence of the "open" conformation in the bovine heart enzyme—cannot be attributed to the presence or absence of Mg^{2+}, as suggested (4). Most likely, the presence of the open conformation in the bovine heart enzyme is caused by the low concentration (and substoichiometric amounts) of ADP in the crystallization medium (14), as demonstrated by recent studies on *Escherichia coli* F_1 (32).

All three α subunits contain bound ATP. Despite the absence of Mg^{2+} in the crystallization medium, the bound nucleotides appear to be ATP-Mg^{2+} (Fig. 5*B*). Because Mg^{2+} and H_2O have the same number of electrons and thus are indistinguishable based on diffraction characteristics, special care was taken to ensure that the additional density observed was indeed Mg^{2+}.

Mechanistic Implications. The three-nucleotide structure reported here suggests a mechanism in which *all* intermediates in the reaction are in one of the two configurations observed in the known crystal structures (bovine–heart, ref. 14; rat–liver, this work). In this mechanism (Fig. 6), which departs significantly from those proposed earlier (4, 6, 14), F_1 configurations of the enzyme with three nucleotides bound play a central role in catalysis whereas species with two nucleotides exist transiently between nucleotide binding and debinding events at physiological nucleotide concentrations. Recent kinetic data on *E. coli* F_1 underscore the importance of full occupancy of catalytic sites for maximal activity (35).

The three β subunits in the rat liver structure are in similar but probably distinct conformations: closed (C with ADP), loose (L with ADP plus P_i), and tight (T with ATP in equilibrium with ADP plus P_i in T′) (Fig. 6). The sites with ADP and P_i represent species poised for the formation of the β-γ phosphate bond. Starting with the most stable species (Fig. 6 species I), ATP synthesis proceeds through a proton translocation-driven conformational change involving the following concerted transformations: T to C, L to T, and C to L. This transformation (I → II; Fig. 6) can only occur when the nucleotide in the tight site is ATP (i.e.,

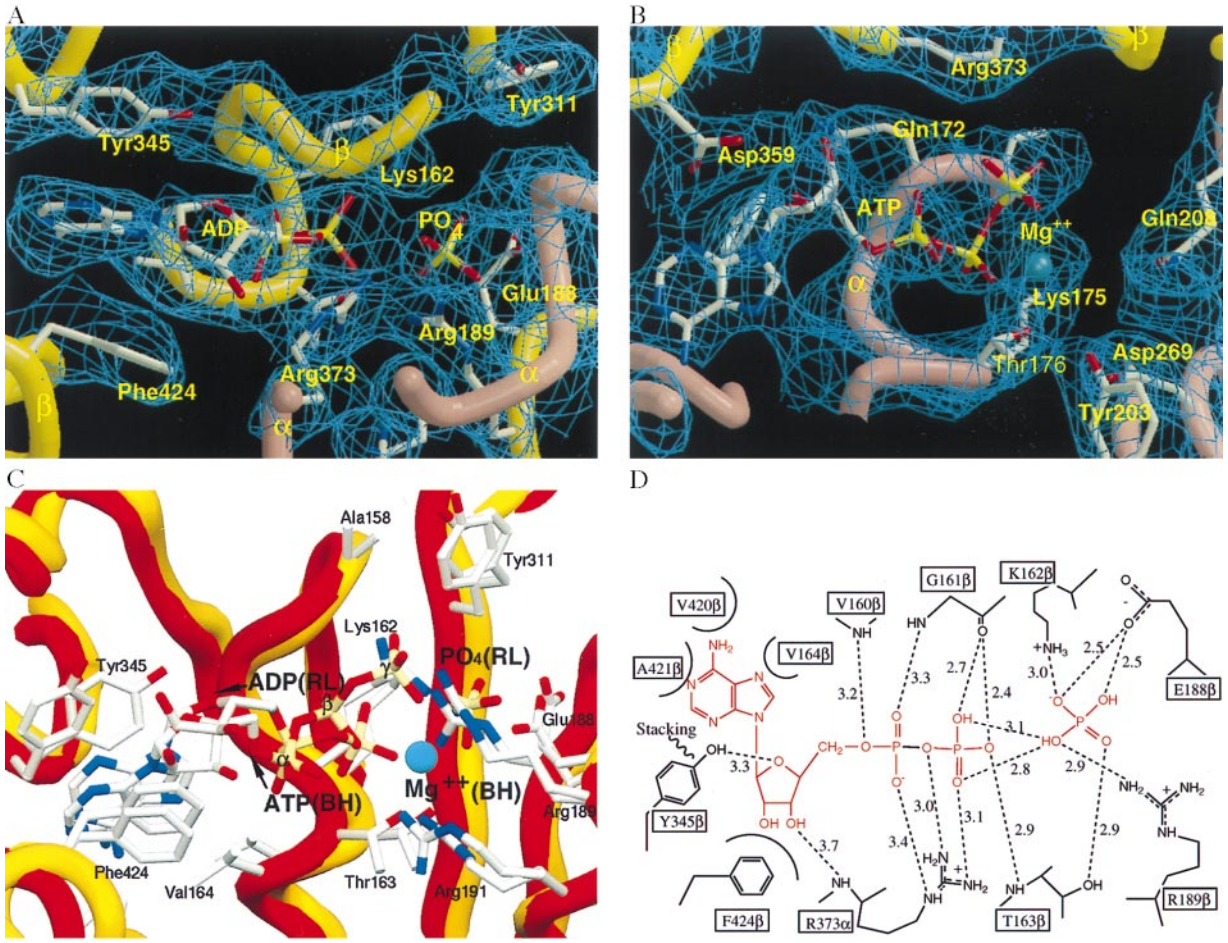

FIG. 5. Nucleotide binding sites of rat liver F_1-ATPase. (*A*) Electron density of the β subunit binding site. The main chain of β is shown in gold, and that of α is shown in rose. Oxygens are red; all other atoms in gray. (*B*) Electron density of α subunit binding site. Color scheme is as in *A*, and Mg^{2+} is in blue. The adenine ring binds in a pocket making van der Waals contacts as well as hydrogen bonding interactions with the protein. Main chain and side atoms provide interactions to the ribose, the phosphates, and the Mg^{2+}. (*C*) Comparison of the β subunit nucleotide binding site of rat liver F_1 (gold) to that of the β_T subunit of bovine heart F_1 (red). (*D*) Schematic diagram of nucleotide binding to the β subunit. Close interactions and hydrogen bonds (with distances in Å) are shown. The ADP and the P_i are shown in red.

T-conformation). Next, ATP is released from the C site with conversion to the O conformation found in subunit β_E of the two nucleotide structure (II → III; Fig. 6). The resulting species has sites in the T, O, and L conformations, with ATP in the T site (in equilibrium with ADP plus P_i in T′ and ADP in the L site. To continue cycling, this species must bind nucleotide. Under physiological conditions, the empty subunit (O site) will bind ADP and return to the C conformation, and P_i will bind to the L site. In this configuration the enzyme is ready for the synthesis of the next ATP. During this portion of the cycle the γ subunit rotates 120°, in coordination with the concerted conformational changes in the major subunits (10). In addition, the conversion of one β subunit from C to O is accompanied by the change in γ described above (pivoting around an axis going though Lys γ 260) that results in its displacement by 4 Å toward the 3-fold axis in the proximity of the DELSEED-containing loop (Fig. 4). Both of these movements are ideal for transmitting changes in the major subunits to the F_0 region of the enzyme.

The forms of the enzyme with T site and T′ site are in fast equilibrium. This equilibrium not only explains the $P_i/H_2{}^{18}O$ exchange data but also the substrate concentration dependence of the exchange in both the hydrolytic and the synthetic directions (reviewed in ref. 4). Under hydrolytic conditions, the extent of incorporation of ^{18}O into P_i increases markedly at low ATP concentrations because the enzyme remains in the form III, with ATP in equilibrium with ADP and P_i until it can bind ATP to the O site. In the synthetic direction, the enzyme remains in the same equilibrium until it binds ADP and P_i, in agreement with data that indicate that exchange increases at low ADP and/or P_i concentrations. The increased exchange observed in the absence of a proton gradient is explained by the equilibrium between the forms containing the T- and T′ sites

The mechanism proposed here involves species containing either two or three nucleotides bound at catalytic sites and no species containing only one in agreement with recent observations that, at physiological concentrations of nucleotides, the predominant F_1-ATPase species contains three bound nucleotides in β subunits (32, 35). By contrast, in some previous proposals (4, 6, 14) in which β subunits proceed sequentially through the tight (T), loose (L), and open (O) conformations (postulated to correspond to the three conformations of the β subunits observed in the two-nucleotide structure—β_T, β_D, and β_E, respectively) (14) F_1-ATPase alternates through species having either one or two nucleotides in catalytic sites per F_1 molecule (4, 6, 14). A recent modification of these proposals that increases the site occupancy in the cycle to include three-nucleotide species (9) is still inadequate because, in contrast to the mechanism proposed here, they require that nucleotides bind and remain bound to β subunits in the O conformation, even though the conformation of the subunit β_E in the two nucleotide structure does not have a well formed nucleotide binding site.

Previous mechanisms have an additional difficulty. With the membrane-bound enzyme operating in the hydrolytic direction, the actual translocation of protons occurs, triggered only by

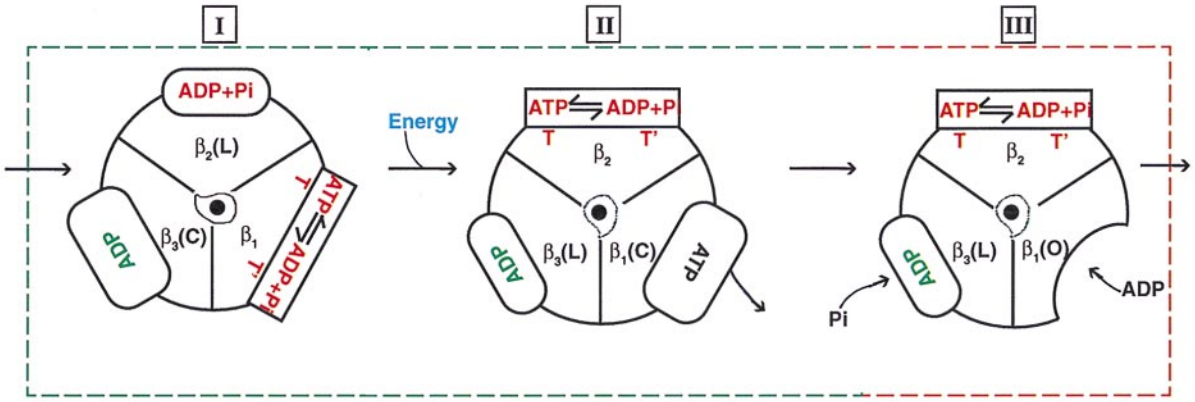

FIG. 6. Proposed mechanism for ATP synthesis/hydrolysis. In the figure, β subunits in one F_1 molecule are labeled β_1, β_2, and β_3. Two configurations of the enzyme are sufficient to describe all of the intermediates in the proposed reaction pathway: (*i*) the three-nucleotide structure with T (tight), L (loose), and C (closed) sites in the β subunits (I and II, boxed by the green dashed line); and (*ii*) the two-nucleotide structure with T, L, and O (open) sites (III, boxed by the red dashed line). Conformations T and T′ of the β subunit are highly similar, but T contains ATP and T′ contains ADP plus P_i. Starting with the most stable species (I), ATP synthesis proceeds through a proton translocation driven conformational change. This transformation (I to II) can occur only with ATP in the T site. Next, ATP is released from the C site which, after release, changes to the O conformation. After intermediate III is reached, the molecule binds ADP in the O site, which immediately changes to the C-conformation, and P_i in the L site becomes species I (but with subunit numbers cyclically permuted). The reaction proceeds cyclically through these steps. Note that, in this mechanism, in contrast to previous proposals (4, 6, 9, 14), the concerted conformational change involving all three β subunits (I to II) occurs in the three nucleotide form of the enzyme and does not involve a β subunit in the open conformation.

binding ATP to the O site and before ATP hydrolysis (4, 6, 9, 14). The driving force is provided by the conformational change that transforms the ATP-occupied O site to a T site. In view of the poor nucleotide binding characteristics of the O site, binding of ATP to the O site appears to be inadequate to trigger the translocation of protons against their concentration gradient. In the mechanism we propose, these concerted conformational changes involve also the hydrolysis of ATP (Fig. 6), providing a more direct coupling between ATP hydrolysis and proton translocation.

The structure of the rat liver F_1-ATPase reported here provides the missing configuration of F_1 necessary to define all intermediates in the reaction pathway of ATP synthesis/hydrolysis. The pathway that results avoids pitfalls of previous proposals and provides a rationale for existing experimental data. The detailed mechanism by which proton translocation through F_0 drives changes in the position of the γ subunit remains the most important enigma in this system. The account of the events occurring in F_1 during ATP synthesis/hydrolysis presented here by providing a step-by-step description of these events places strong constraints on how this coupling actually can occur.

We thank Drs. J. Berg, D. Leahy, and J. Wehrle for critical reading of the manuscript, Dr. Y. H. Ko for valuable help and suggestions, and Dr. N. Carrasco for critical comments and continuous encouragement. Synchrotron data were collected at the National Synchrotron Light Source (Brookhaven National Laboratory) line X25 and Howard Hughes Medical Institute beamline X4A; we thank Dr. Craig Ogata for help and guidance at the line. We thank the National Cancer Institute, Frederick, Super Computing Facility for allocation of computing time. Equipment used in this work was purchased and supported with funds from the National Science Foundation, National Institutes of Health, the Keck Foundation, and the Lucile P. Markey Charitable Trust. This work was supported by National Institutes of Health Grants CA 10951 (to P.L.P.) and GM 25432 (to L.M.A.). This article is dedicated to the memory of Dr. Albert L. Lehninger, whose enthusiasm, interest, and encouragement were a constant source of inspiration.

1. Catterall, W. A. & Pedersen, P. L. (1971) *J. Biol. Chem.* **246,** 4987–4994.
2. Catterall, W. A., Coty, W. A. & Pedersen, P. L. (1973) *J. Biol. Chem.* **248,** 7427–7431.
3. Catterall, W. A. & Pedersen, P. L. (1974) *Biochem. Soc. Spec. Publ.* **4,** 63–88.
4. Boyer, P. D. (1997) *Annu. Rev. Biochem* **66,** 714–749.
5. Weber, J. & Senior, A. E. (1997) *Biochim. Biophys. Acta* **1319,** 19–58.
6. Cross, R. L. (1981) *Annu. Rev. Biochem.* **50,** 681–714.
7. Pedersen, P. L. & Amzel, L. M. (1993) *J. Biol. Chem.* **268,** 9937–9940.
8. Cross, R. L., Cunningham, D. & Tamura, J. K. (1984) *Curr. Top. Cell. Regul.* **24,** 365–378.
9. Duncan, T. M., Bulygin, V. V., Zhou, Y., Hutcheon, M. L. & Cross, R. L. (1995) *Proc. Natl. Acad. Sci. USA* **92,** 10964–10968.
10. Noji, H., Yasuda, R., Yoshida, M. & Kinosita, K., Jr. (1997) *Nature (London)* **386,** 299–302.
11. Sabbert, D., Engelbrecht, S. & Junge, W. (1996) *Nature (London)* **381,** 623–623.
12. Capaldi, Q. A., Aggeler, R., Wilkens, S. & Grüber, G. (1996) *Biochem. Biophys. Acta* **28,** 397–402.
13. Futai, M. & Amote, H. (1996) *J. Bioenerg. Biomembr.* **28,** 409–414.
14. Abrahams, J. P., Leslie, A. G. W., Lutter, R. & Walker, J. E. (1994) *Nature (London)* **370,** 621–628.
15. Amzel, L. M. & Pedersen, P. L. (1978) *J. Biol. Chem.* **253,** 585–597.
16. Lutter, R., Abrahams, J. R., van Raaij, M. J., Leslie, A. G., Walker, J. E. (1993) *J. Mol. Biol.* **229,** 787–790.
17. Bianchet, M., Ysern, X., Hullihen, J., Pedersen, P. L. & Amzel, L. M. (1991) *J. Biol. Chem.* **266,** 21197–21201.
18. Pedersen, P. L. & Hullihen, J. (1978) *J. Biol. Chem.* **253,** 2176–2183.
19. Otinowski, Z. (1993) in *Proceedings of the CCP4 Study Weekend: Data Collection and Processing,* eds. Sawyer, L., Isaacs, N. & Bailey, S. (SERC Daresbury Laboratory, Warrington, United Kingdom), pp. 56–62.
20. Redimbo, M. R. & Yeats, T. O. (1993) *Acta Crystallogr. D* **49,** 375.
21. SERC Collaborative Computional Project No. 4 (1994) *Acta Crystallogr. D* **50,** 760–776.
22. Jones, T. A., Zou, J. Y., Cowan, S. W., Kjeldgaard, M. (1991) *Acta Crystallogr. A* **47,** 110–119.
23. Brünger, A. T. (1992) *XPLOR Version 3.1: A System for X-ray Crystallography and NMR* (Yale Univ. Press, New Haven, CT.
24. Evans, S. V. (1993) *J. Mol. Graphics* **11,** 134–138.
25. Kraulis, P. J. (1991) *J. Appl. Crystallogr.* **24,** 946–950.
26. Bacon, D. J. & Anderson, W. F. (1988) *J. Mol. Graphics* **6,** 219–220.
27. Merrit, E. A. & Murphy, M. E. P. (1994) *Acta Crystallogr. D* **50,** 869–873.
28. Garboczi, D. N., Fox, A. H., Gerring, S. L. & Pedersen, P. L. (1988) *Biochemistry* **27,** 553–560.
29. Lee, J. H., Garboczi, D. N., Thomas, P. J. & Pedersen, P. L. (1990) *J. Biol Chem.* **265,** 4664–4669.
30. Amzel, L. M., Bianchet, M. A. & Pedersen, P. L. (1992) *J. Bioenerg. Biomembr.* **24,** 429–433.
31. Bianchet, M. A., Medjahed, D., Hullihen, J., Pedersen, P. L. & Amzel, L. M. (1994) *Biochim. Biophys. Acta* **1187,** 163–164.
32. Lobau, S., Weber, J. & Senior, A. E. (1997) *FEBS Lett.* **404,** 15–18.
33. Shirakihara, Y., Leslie, A. G., Abrahams, J. P., Walker, J. E., Ueda, T., Sekimoto, Y., Kambara, M., Saika, K., Kagawa, Y. & Yoshida, M. (1997) *Structure* **5,** 825–836.
34. Pedersen, P. L., Hullihen, J., Bianchet, M. A., Amzel, L. M. & Lebowitz, M. S. (1995) *J. Biol. Chem.* **270,** 1775–1784.
35. Lobau, S., Weber, J., Wilke-Mounts, S. & Senior, A. E. (1996) *J. Biol. Chem.* **272,** 3648–3656.